ANALYSIS OF NEOs REACHABILITY WITH NANO-SATELLITES AND LOW-THRUST PROPULSION

Cristian Greco[1], **Marilena Di Carlo**[1], **Lewis Walker**[1], and **Massimiliano Vasile**[1]

[1] *Department of Mechanical and Aerospace Engineering, University of Strathclyde, 75 Montrose Street, G1 1XJ, Glasgow, United Kingdom, +44 (0) 141 548 5161,*
{ c.greco , marilena.di-carlo , lewis.walker , massimiliano.vasile }@strath.ac.uk

ABSTRACT

This paper presents an analysis of new potential space missions to Near Earth Objects (NEOs) using nano-satellites and low-thrust propulsion. Both rendezvous and flyby scenarios are examined over a launch window that goes from 2024 to 2034. The paper first investigates the reachability of thousands of sample asteroids taken from the existing database of NEOs. Then, a sensitivity analysis is performed on a large number of transfers to study the effect of uncertainty on the initial mass at launch, thrust level and specific impulse of the engine. This second step provides information on the required spacecraft system and it is used to perform a more detailed trajectory optimisation on a selected scenario to study the effect of uncertain boundary conditions and disturbance on the control. Finally, an analysis is performed to assess how to improve our knowledge of some asteroid attributes during a flyby by using sensors that can be installed on board a nano-satellite.

1 INTRODUCTION

In recent years, the exploration of Near Earth Objects (NEOs) has attracted substantial attention in the scientific community. The orbital elements, physical and chemical characteristics of these objects are, in fact, known only with limited levels of accuracy. Moreover, many NEOs are classified as potentially hazardous, and could pose a threat to our planet. So far, few missions have targeted Near Earth Objects[1] [1, 2, 3, 4]. JAXA's Hayabusa 2[2] and NASA's OSIRIS-REx[3] are currently travelling towards their targeted NEOs, and plan to reach them in July and August 2018, respectively. The known population of NEOs includes over 18000 objects, and so the fraction of objects visited by a space mission is extremely limited.

Nano-satellites represent a valid alternative to traditional spacecraft, as they are cabable of low-cost, fast, and efficient exploration of NEOs. NASA has recently proposed NEO Scout[4], a 6U CubeSat secondary payload mission, aimed at visiting an asteroid of the NEO population. Considering the limited mass resources of nano-satellites, an efficient propulsion technology would be required for an interplanetary mission that uses this platform. In this regard, low-thrust propulsion systems provide lower propellant consumption than high-thrust propulsion technologies.

[1] https://cneos.jpl.nasa.gov/
[2] http://global.jaxa.jp/projects/sat/hayabusa2/
[3] https://www.nasa.gov/osiris-rex
[4] https://www.nasa.gov/content/nea-scout

For interplanetary missions using nano-satellites and small platforms characterised by limited resources and capabilities, it is extremely important to account for uncertainties during the mission design process. In the early phase of the design of a space mission, in fact, the values of several design parameters might be either unknown or known with a degree of uncertainty [5]. An insufficient consideration for uncertainty, in this phase, would lead to a wrong decision on the feasibility of the whole mission.

This paper presents an analysis of the reachability of NEOs, using a low-thrust propelled nano-spacecraft, and considering two possible scenarios: rendezvous and flyby. The study is performed over a lunch window that goes from 2024 to 2034 and includes objects of scientific interest and potentially hazardous objects. Sensitivity and uncertainty analyses are performed to assess the impact of uncertain system parameters, boundary conditions and disturbances in the control.

The paper is structured as follow. Section 2 introduces the proposed mission scenarios. The reachability analysis using rendezvous, and the sensitivity and uncertainty analyses are described in Section 3. The flyby scenarios are described in Section 4, while Section 5 presents the analysis of the remote sensing during flyby. Finally, Section 6 concludes the paper.

2 DEFINITION OF MISSION SCENARIOS

A small celestial object is classified as a NEO if it has a perihelion smaller than 1.3 AU[1]. Currently, around 18000 Near Earth Asteroids (NEAs) and 107 Near Earth Comets (NECs) have been discovered. Among these, 888 NEAs have an estimated diameter roughly larger than 1 km, and 1899 are considered Potentially Hazardous Asteroids (PHAs), based on their Earth Minimum Orbit Intersection Distance ($MOID \leq 0.05$ AU) and their estimated diameter. In 2001, Perozzi et al. [6] shortlisted 60 scientifically interesting asteroids with peculiar traits, while NASA[5] and ESA[6] maintain a list of PHAs. For the current study, the main goal is to acquire more information about PHAs and improve our knowledge of their ephemerides. The ideal solution would be to rendezvous with a large number of potentially interesting targets. Therefore, the first scenario we will investigate is a single rendezvous with objects within these lists. The use of small, cheap platforms would potentially allow reaching multiple targets for a cost comparable to a single large scale mission. On the other hand, most NEOs have high eccentricity and inclination, which would make rendezvous extremely challenging, even using low-thrust propulsion. For this reason, we also consider a second mission scenario: the single flyby of several NEOs at their ascending or descending nodes. For both scenarios, a standard 12U spacecraft with an initial mass m_0 of 24 kg is considered. The spacecraft is equipped with a solar electric propulsion (SEP) engine with a specific impulse I_{sp} of 1200 s and a thrust level that follows the inverse square law:

$$T(r) = \frac{T_{1AU}}{(r/\tilde{r})^2} \tag{1}$$

where T_{1AU} is the thrust at 1 AU, and $\tilde{r} = 1$ AU. The thrust level at 1 AU is assumed to be $T_{1AU} = 0.006$ N. The values of the thrust level and specific impulse are based on the characteristics of the HT-100 Hall Effect Thruster[7].

3 RENDEZVOUS SCENARIOS

In this study, we estimate the optimal ΔV cost and time of flight to rendezvous with 7310 different NEOs with a wide range of orbital parameters, including the objects reported in [6] and those from

[5] https://cneos.jpl.nasa.gov/sentry/

[6] http://neo.ssa.esa.int/risk-page

[7] www.sitael.com/wp-content/uploads/2015/10/HT-100.pdf

the ESA and NASA risk lists; the considered launch window spans the period from 01/01/2024 to 31/12/2034. The search space, defined by departure date, time of flight and number of revolutions, has been discretized with a uniform grid. The departure date T_{dep} was discretised with a time step of 20 days, the time of flight ToF, spanning 200-1000 days, was discretised with a time step of 20 days, and the number of revolutions n_{rev} was discretised with unit steps in the range from 0 to 4. The ΔV was estimated using the spherical shaping method [7], with no constraint on the maximum thrust level. For each of the 7310 NEOs, a trajectory was calculated for all departure dates, transfer times and number of revolutions. As an example, Figure 1 shows the resulting ΔV for asteroid 2000 SG_{344}; T_{dep}-ToF regions of favourable ΔVs are evident.

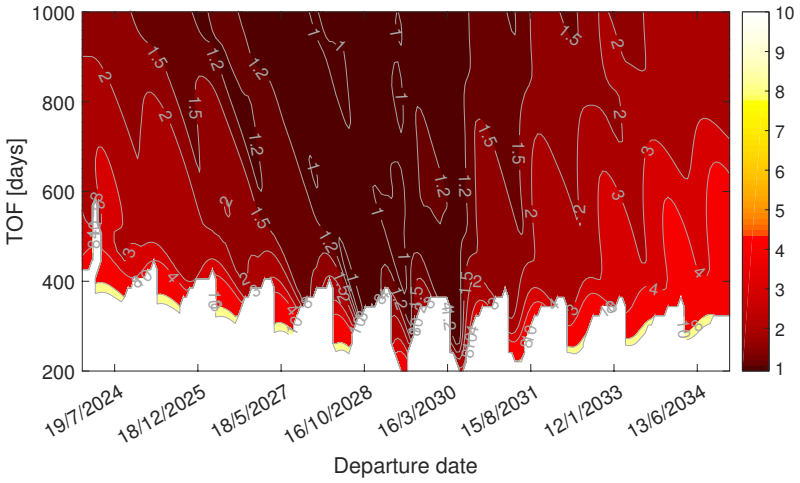

Figure 1: Porkchop plot for asteroid 2000 SG_{344} displaying ΔV for different values of T_{dep} and ToF.

From this analysis, the 50 most promising solutions for each asteroid were saved in a database.

Figure 2 shows the *a-e* map, of respectively target semi-major axis and eccentricity, and the *a-i* map, of target semi-major axis and inclination, created using the best ΔV rendezvous for each NEO.

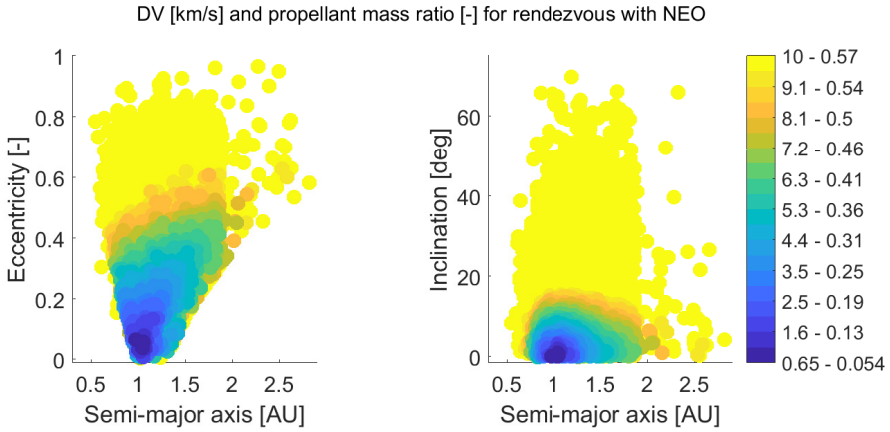

Figure 2: Map of the best ΔV solutions of the database plotted against target semi-major axis and eccentricity (left), and target semi-major axis and inclination (right). The colorbar levels indicate both the ΔV [km/s] and the corresponding propellant mass ratio for the reference value of I_{sp}.

Results show that the ΔV is lower for asteroids with semi-major axis close to 1 AU, and eccentricity and inclination close to 0, since these are the orbital elements of the Earth. In addition, these maps illustrate how rendezvous trajectories to significantly eccentric and inclined orbits, e.g. $e < 0.4$ and $i < 15$ deg, are still feasible with a moderate propellant consumption. For highly eccentric and inclined

orbits, the matching condition on the target velocity requires a critical propellant mass ratio regardless of the semi-major axis value.

Table 1 lists the 8 NEOs with the lowest ΔV requirement for rendezvous. Although the propellant mass ratio is small, none of these are in the list of scientifically relevant NEAs reported in [6].

Table 1: List of NEOs rendezvous with smallest ΔV. The table reports the semi-major axis a, eccentricity e, inclination i and absolute magnitude H of the target asteroid, as well as the departure date, time of flight, ΔV and propellant ratio m_p/m_0 for the corresponding rendezvous.

Name	a [AU]	e [-]	i [deg]	H [-]	T_{dep} [date]	ToF [day]	ΔV [km/s]	m_p/m_0 [-]
2018 AV_2	1.045	0.041	0.123	28.7	04/09/2032	302.6	0.655	0.054
2014 WX_{202}	1.036	0.059	0.413	29.6	23/11/2032	446.2	0.852	0.070
2000 SG_{344}	0.977	0.067	0.112	24.7	22/08/2028	364.1	0.923	0.075
2012 TF_{79}	1.050	0.038	1.005	27.4	07/10/2025	815.4	1.021	0.083
2010 UE_{51}	1.055	0.060	0.624	28.3	11/10/2034	876.9	1.072	0.087
2007 UN_{12}	1.054	0.061	0.236	28.7	24/07/2033	302.5	1.205	0.097
2008 EA_9	1.059	0.080	0.425	27.7	28/11/2030	446.2	1.213	0.098
2017 SV_{19}	1.063	0.040	1.306	25.0	24/12/2027	876.9	1.301	0.105

However, these asteroids are deemed to be interesting for the following reasons:

- 2000 SG_{344} is among the 4 objects with highest Palermo Scale (PS) on the the ESA risk list[6], and one of the top 10 objects in the NASA impact risk list[5] [8];
- 2010 UE_{51} has been studied for the asteroid deflection demonstration mission SIROCO [9];
- 2000 SG_{344}, 2010 UE_{51}, 2007 UN_{12} and 2008 EA_9 are labelled as Easily Retrievable Objects and considered candidates for an asteroid retrieval mission [10];
- 2000 SG_{344} is a candidate of a threat mitigation demonstrator[8] and a NASA manned mission[9];
- 2000 SG_{344} and 2017 SV_{19} are, respectively, the first and third most promising targets within the Near-Earth Object Human Space Flight Accessible Targets Study (NHATS)[1].

From this analysis, 2000 SG_{344}, an Aten asteroid with 20-100 m diameter, was selected as a reference case because of the optimal trade-off between propellant consumption and potential mission outcomes.

3.1 Optimisation of Rendezvous Transfers

For each asteroid, the minimum ΔV trajectory from the shaping method was re-optimised using a tool called FABLE (Fast Analytical Boundary-value Low-thrust Estimator) [11]. FABLE transcribes the optimal control problem using a single shooting approach in which the transfer from the Earth to each asteroid is segmented into a sequence of coast and thrust arcs. The starting point of the i-th thrust arc is defined by the true longitude L_i, while its length is defined by the angle ΔL_i. The thrust direction is defined on each thrust arc by a constant azimuth angle in the RTN reference frame, α_i. The elevation angle β_i is equal to zero since the flybys are realised at the nodal point of the asteroids' orbit, and therefore no out-of-plane maneuvers are required. On each thrust arc, the thrust magnitude follows the inverse square law described in Equation 1. The motion of the spacecraft subject to low-thrust acceleration is analytically propagated in non-singular equinoctial elements, using a first-order expansion in the perturbing acceleration [12].

[8] http://www.jb.man.ac.uk/meetings/nam2012/archive/PL1/Fitzsimmons.pdf
[9] https://www.nasa.gov/pdf/604310main_4-GER_WS_Near-Term-Asteroids-Hopkins.pdf

For each asteroid, the best solution obtained with the shaping method defines a departure date T_{dep} and time of flight ToF; using FABLE, the optimal ΔV for the rendezvous was obtained by solving the following non-linear programming (NLP) problem:

$$\begin{aligned} &\min_{\mathbf{u}\in\mathbb{U}} \ \Delta V(\mathbf{u},\ \bar{\boldsymbol{\xi}},\ T_{dep},\ T_{dep}+ToF) \\ &\text{s.t. } \mathbf{c}\left(\mathbf{u},\ \bar{\boldsymbol{\xi}},\ T_{dep},\ T_{dep}+ToF\right)=0 \end{aligned} \tag{2}$$

where $\mathbf{u}\subset\mathbb{R}^{n_u}$ is the vector of optimisation variables, and $\bar{\boldsymbol{\xi}}=[m_0,\ I_{sp},\ T_{1AU}]^T$ is the vector of the nominal design parameters of the system. The objective function is (refer to Equation 1):

$$\Delta V=\int_{T_{dep}}^{T_{dep}+ToF}\frac{T\left(r(\mathbf{u})\right)}{m(t)}dt \tag{3}$$

and is computed analytically. The equality constraints $\mathbf{c}$ are used to impose that the state vectors $\mathbf{X}=[\mathbf{r},\mathbf{v}]^T$ of spacecraft and asteroid match at the rendezvous:

$$\mathbf{c}=\mathbf{X}_{ast}(T_{dep}+ToF)-\mathbf{X}_{SC}(\mathbf{u},\ \bar{\boldsymbol{\xi}},\ T_{dep}+ToF) \tag{4}$$

The NLP problem was solved using Matlab *fmincon-sqp*. Figure 3 shows a comparison of the ΔV obtained using the shaping method (blue circles) and using FABLE (red and green dots). The transfers are sorted from those with lower ΔV to those with higher ΔV, and only the first 5000 sorted solutions are shown in the plot. Green and red dots are used to represent, with different colors, solutions of the shaping method characterised by different conditions of the shaping solution peak thrust with respect to the nominal thrust T_{1AU}. In particular, if $T_{sh}(r)$ is the thrust profile of the shaping method along the entire transfer, the peak thrust T_{peak} is defined as (refer to Equation 1):

$$T_{peak}=\max\left[\left(\frac{r}{\tilde{r}}\right)^2 T_{sh}(r)\right] \tag{5}$$

The solutions of FABLE for which $T_{peak}<T_{1AU}$ are represented by green dots in Figure 3, while the red dots are used to represent the solution for which $T_{peak}>T_{1AU}$. Results show that when $T_{peak}<T_{1AU}$, FABLE found solution with lower ΔV than those of the shaping method. Out of the 7310

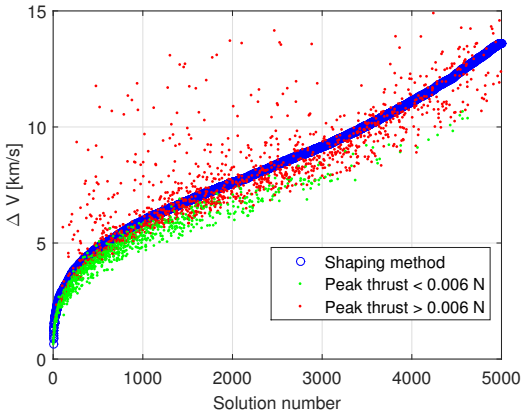

Figure 3: Comparison of the ΔV cost of different rendezvous using spherical shaping or FABLE.

rendezvous, 866 cases had an estimated peak thrust lower than the set threshold, $T_{peak}<T_{1AU}$. In all these cases FABLE provided an improved solution with an averaged 11% gain in ΔV. The left bottom area of Figure 3 also shows that when we restrict the analysis only to solutions with reasonable values of ΔV, the shaping method gives more reliable indications on the ΔV of the transfer; in particular, approximately 90% of the solutions generated by the shaping method could be improved by FABLE when $\Delta V_{sh}\leq 5.5$ km/s.

3.2 Rendezvous Sensitivity Analysis

In this section, a sensitivity analysis is performed on the rendezvous database to compute the reachable set of asteroids, when a variability in the system design is considered. In particular, we considered the uncertain vector $\boldsymbol{\xi} = [m_0,\ I_{sp},\ T_{1AU}]^T$ that can take values within the uncertain space Ω, defined by the lower and upper bounds $\boldsymbol{\xi}^L = [19.2,\ 1080,\ 0.005]^T$ and $\boldsymbol{\xi}^U = [28.8,\ 1320,\ 0.007]^T$.

Within Ω, 200 samples were generated by Halton sequence [13], and for each sample $\boldsymbol{\xi}_h \in \Omega$, the top 10 best-$\Delta V$ combinations of departure time, time-of-flight and revolution number were re-evaluated with the sampled value of system parameters. Then, for each NEO rendezvous, a trajectory was labelled feasible if it satisfied the constraint on the maximum thrust, i.e. $T_{peak} < T_{1AU}$ (see Equation 5), and if the propellant mass ratio satisfied the condition $m_p/m_0 \leq 0.45$, where m_p is the propellant mass. The reachable sets corresponding to the samples with largest, intermediate and smallest percentage of feasible transfers are plotted in Figure 4.

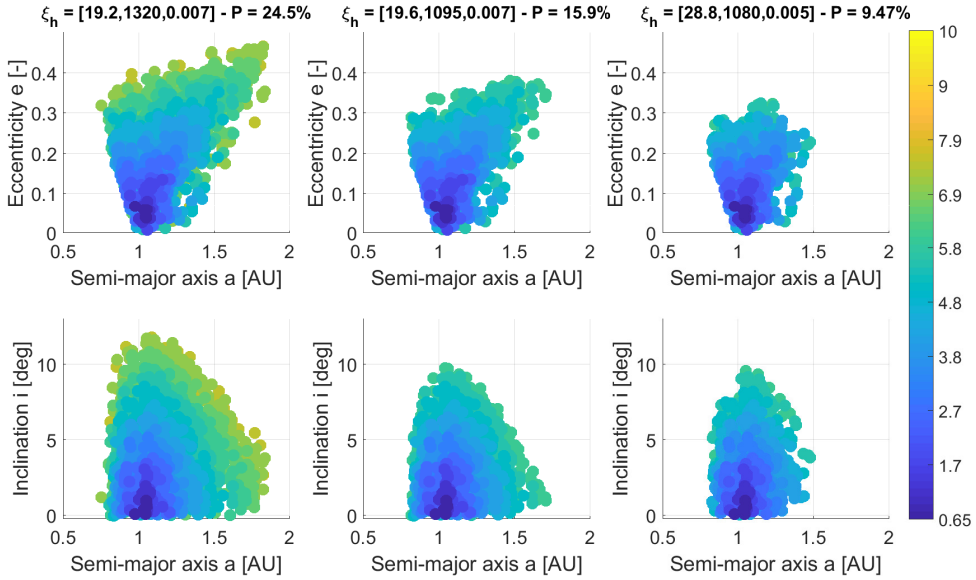

Figure 4: Reachable sets of samples with largest (left), intermediate (center) and smallest (right) percentage of feasible transfers against target semi-major axis and eccentricity (top), and target semi-major axis and inclination (bottom). On top of each group of subplots, the sample value is reported, while P is the percentage of feasible trajectories. The colorbar indicate the ΔV levels.

Results confirm that higher values of T_{1AU} are favourable as they allow for trajectories with higher peak thrust, a convenient characteristic especially when the target asteroid has a semi-major axis considerably larger than 1 AU. Similarly, a higher value of specific impulse I_{sp} results in lower propellant mass consumption, hence increasing the number of rendezvous that satisfy the propellant mass ratio condition. The initial mass does not influence the latter condition, but does affect the maximum thrust constraint. Indeed, for a given control acceleration, the required thrust is directly proportional to the spacecraft mass. Therefore, a lower initial mass is preferable. Although the best-case and worst-case samples fall on two vertices of the uncertain space Ω, the extent of the reachable set does not vary monotonically with all the uncertain system parameters. This effect stems from the conflicting effects of the specific impulse on the two feasibility conditions. Indeed, while a higher I_{sp} reduces the propellant mass consumption, it also directly results in a bigger instantaneous mass of the spacecraft, which therefore causes an increased thrust peak for an equal control acceleration profile. To better visualise this double contribution, Figure 5 shows how the introduction of the condition $m_p/m_0 < 0.45$ shifts the best sample from the vertex corresponding to the lowest value of I_{sp} in the cube represent-

ing Ω (a situation when lower I_{sp} values actually help in decreasing the peak thrust), to the vertex corresponding to the highest I_{sp}, when higher values result in a reduction of the propellant mass ratio.

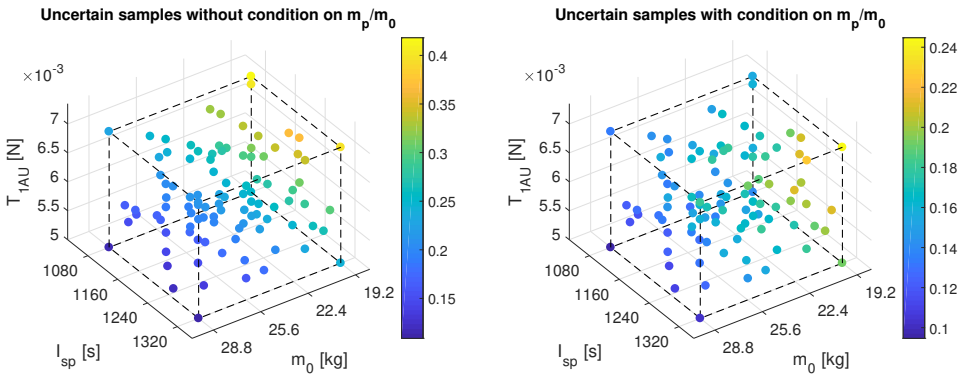

Figure 5: Uncertain samples for different values of m_0, I_{sp} and T_{1AU}. The colorbar levels indicate the percentage of feasible NEO rendezvous when only the maximum peak thrust condition (see Equation 5) is enforced (left), and when also the limit condition on maximum m_p/m_0 is considered (right).

3.3 Uncertainty Analysis for Rendezvous with Asteroid 2000 SG_{344}

In this section, an uncertainty quantification analysis is applied to the rendezvous with asteroid 2000 SG_{344}. Two cases are considered: the quantification of the impact of uncertain system parameters $\boldsymbol{\xi}$ and the quantification of the impact on boundary conditions and control profile. In the former case FABLE is used to determine the nominal control $\bar{\mathbf{u}}$ required to realise the rendezvous when using the nominal values of the system parameters, $\bar{\boldsymbol{\xi}}$, defined in Section 2, while in the latter case a higher fidelity multiple-shooting approach is used with a full numerical integration of the dynamics.

The optimal nominal trajectory to 2000 SG_{344} is shown in Figure 6. The ΔV required for the rendezvous is $\Delta V_{FABLE} = 0.7999$ km/s (refer to Table 1 for the corresponding ΔV of the shaping method), corresponding to a propellant mass of 1.6081 kg.

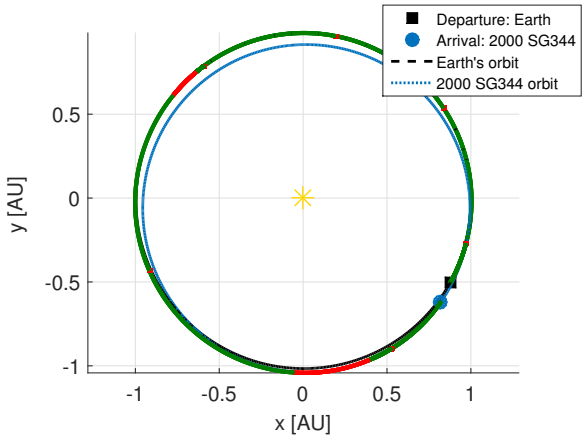

Figure 6: Optimised rendezvous transfer to asteroid 2000 SG_{344}. Coast arcs are shown in green and thrust arcs are shown in red.

3.3.1 Uncertainty Quantification on System Parameters

It is assumed that the system parameters m_0, I_{sp} and T_{1AU} are uncorrelated independent stochastic variables with probability distribution defined by three probability-boxes, or p-boxes [14]. The p-boxes are modelled with Bernstein polynomials of order 3 [15]. In this work the aim is to study the

lower expectation of a condition $g < \bar{g}$, $E_l[g < \bar{g}]$. The lower expectation of $g < \bar{g}$ is the solution of the following linear optimisation problem:

$$E_l(g < \bar{g}) = \min_{\mathbf{c} \in \mathscr{C}} \int_{\bar{\Omega}} p_{\mathbf{c}}(\boldsymbol{\xi})\, d\boldsymbol{\xi} \tag{6}$$

where $\bar{\Omega} = \{\boldsymbol{\xi} \in \Omega \mid g(\overline{\mathbf{u}}, \boldsymbol{\xi}) < \bar{g}\}$ and $p_c(\boldsymbol{\xi})$ is the multivariate lower probability [15]. In particular, the aim is to study the following lower expectations, under the uncertainties associated with the system parameters:

$$E_l(m_p < \bar{m}_p) \;,\; E_l\left(\Delta r < \bar{\Delta r}\right) \;,\; E_l\left(\Delta v < \bar{\Delta v}\right) \tag{7}$$

In the previous equations m_p is the mass of propellant, $\Delta r = \|\mathbf{r}_{SC}(\mathbf{u}, \boldsymbol{\xi}, t_0 + ToF) - \mathbf{r}_{ast}(t_0 + ToF)\|$ and $\Delta v = \|\mathbf{v}_{sc}(\mathbf{u}, \boldsymbol{\xi}, t_0 + ToF) - \mathbf{v}_{ast}(t_0 + ToF)\|$. The computation of the lower expectation is realised solving a linear programming problem [15].

Results for the lower expectation of the propellant mass are shown on the left in Figure 7, for different values of $\bar{m}_p$, reported on the x axis of the plot. With the nominal values of the uncertain parameters, the mass of propellant required to realise the transfer is 1.6081 kg. Results in Figure 7 show that in the range of considered values for $\boldsymbol{\xi}$, and using the nominal control for the transfer, the lower expectation on this value of propellant mass is approximately 0.014. A lower expectation equal to 1 is reached for a value of propellant mass equal to 2.08 kg, while lower expectation equal to 0 is obtained for a value of the propellant mass equal to 1.5 kg. This means that a minimum propellant mass of 1.5 kg has to be accounted for under the considered uncertainties. However, only a value of 2.08 kg of propellant mass guarantees that the rendezvous can be realised under any considered uncertainty. Figure 7 shows, on the centre and right, the lower expectation on the satisfaction of the position and velocity constraints, for different values of $\bar{\Delta r}$ and $\bar{\Delta v}$, reported on the x axis. The lower expectation is equal to 1 for values of constraint violation greater than $2.50 \cdot 10^6$ km for the position and 0.3 km/s for the velocity.

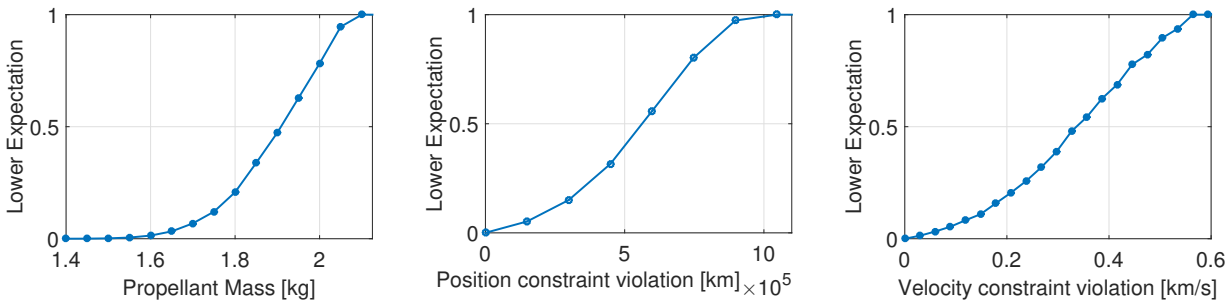

Figure 7: Lower expectation on the satisfaction of the position and velocity constraint violation for the rendezvous with asteroid 2000 SG_{344}.

3.3.2 Control Robustness and Reliability Assessment

This section considers the effects of uncertainty on boundary conditions and control profile. In particular, the uncertain parameters are: the initial spacecraft velocity, namely its magnitude, v_{dep}, and two angles describing its direction, α and δ, to account for possible launcher orbit injection errors; the target final state, described in terms of Keplerian orbital elements; two model parameters, A and w, that describe a fluctuating disturbance on the controlled thrust level $\mathbf{u}_c$, affecting therefore the actual thrust value as:

$$\mathbf{u}(t) = (1 + A \sin wt)\, \mathbf{u}_c(t) \tag{8}$$

The uncertain space is now defined by deviations $\pm\boldsymbol{\xi}_{dev}$ with respect to reference value $\boldsymbol{\xi}_{ref}$ (as considered in previous analyses) as reported in Table 2, where the symbol $\oplus$ identifies the corresponding state values of the Earth at departure time. The values of orbital element deviations are set as 3-σ uncertainties, according to the data from the JPL Small-Body Database[10].

Table 2: Reference value and deviations of the uncertain dynamical parameters.

	v_{dep} [km/s]	α [deg]	δ[deg]	a [AU]	e [-]	i [deg]	Ω [deg]	ω [deg]	M_0 [deg]	A [-]	w [rad/s]
$\boldsymbol{\xi}_{ref}$	$v_\oplus$	$\alpha_\oplus$	$\delta_\oplus$	0.98	0.07	0.11	191.95	275.31	299.77	0	5.3e-2
$\boldsymbol{\xi}_{dev}$	0.1	1.5	1.5	1.2e-6	6.1e-6	1.5e-5	2.4e-3	2.4e-3	1.2e-2	0.1	5.2e-2

This uncertain space is sampled by a sparse grid scheme of level 3, using Gauss-Patterson nodes [16], which generates 2575 samples. For each sample, a full trajectory optimisation is carried out using a direct variational multiple shooting transcription [17] to generate an optimal and feasible control law.

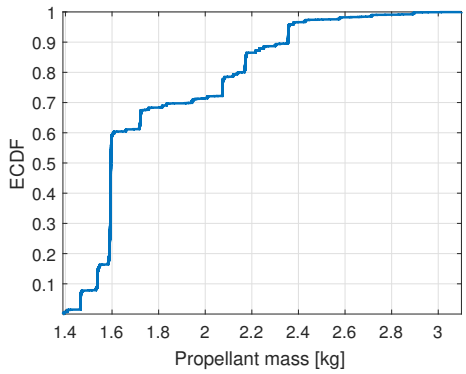

Figure 8: Experimental cumulative distribution function on the propellant mass for rendezvous with asteroid 2000 SG_{344} generated by a sparse grid sampling in the uncertain space defined in Table 2.

Figure 8 shows the empirical cumulative distribution function (ECDF) for the propellant mass. There is a 0.6 probability to have a mass consumption smaller or equal than 1.6 kg, the peak value in the associated probability distribution. The full propellant mass range of this mission scenario spans from 1.38 kg to 3.09 kg, a wider interval than the ones coming from the uncertainty in system parameters only. Note that all the control profiles fully respect the constraint on the maximum thrust level and allow meeting the terminal constraints. Hence, this analysis provides a further indication of the propellant mass margins to be taken into account during early phases of the mission concept for these uncertain scenarios.

4 FLYBY SCENARIOS

Flybys are realised at the nodal points to avoid expensive changes of orbital elements. The computation of flyby transfers are performed for a total of 677 asteroids, divided into three groups: 86 NEOs taken from the ESA and NASA risk lists (Section 2), 60 NEOs of scientific interest [6], and an additional 531 NEOs with nodal point distance from the Sun, r_{node}, between 0.7 and 1.3 AU. Different departure dates between 1 January 2024 and 31 December 2034 are considered (Section 3), with a time step of 45 days. The time of flight for each transfer depends on the considered departure date and on the time of passage of the asteroid at its nodal point. Times of flight in the range from 200 to 1000 days are considered.

[10]https://ssd.jpl.nasa.gov/sbdb.cgi?sstr=2000SG344;cad=1

For each combination of departure date T_{dep} and time of flight ToF, the optimal ΔV of the transfer is obtained using FABLE (Subsection 3.1), solving a NLP problem formulated as in Equation 2. The equality constraint is now formulated as

$$\mathbf{c} = \mathbf{r}_{ast}(T_{dep} + ToF) - \mathbf{r}_{SC}(\mathbf{u}, \boldsymbol{\xi}, T_{dep} + ToF) \tag{9}$$

in order to impose matching of the position vectors of spacecraft and asteroid at flyby.

As an example, Figure 9 shows the ΔV for the flyby of asteroid 2004 MN_4 for different departure dates and arrival dates at the nodal points, and $\Delta V < 10$ km/s.

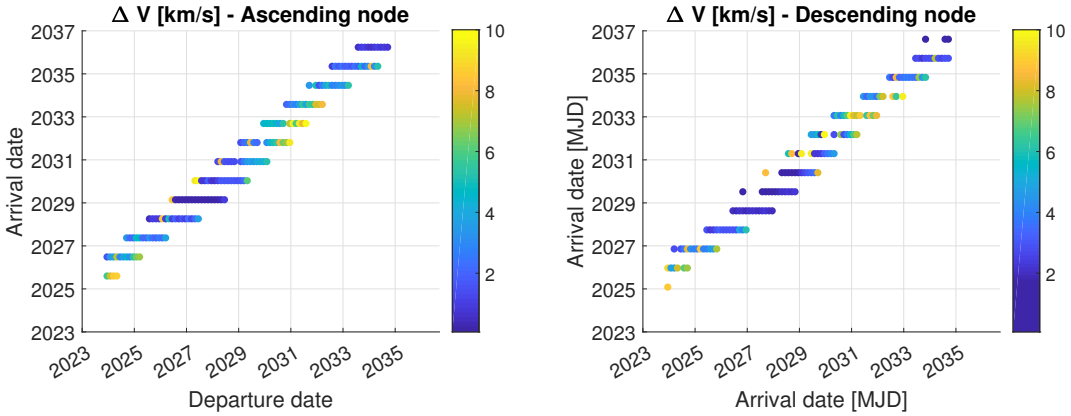

Figure 9: ΔV for flyby to the ascending and descending nodes of asteroid 2004 MN_4.

Figure 10 shows the minimum ΔV required to realise a flyby as a function of the distance from the Sun of the nodal point where the flyby takes place, r_{node}. Asteroids belonging to different groups are identified by different markers. The results in Figure 10 show that a dependence of the ΔV on

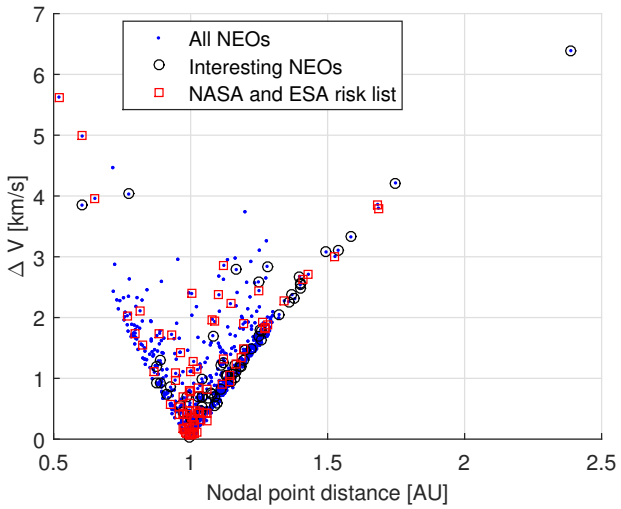

Figure 10: Relationship between distance from the Sun of the node where the flyby takes place and the required ΔV.

the nodal point distance from the Earth (1 AU) is not always verified (the points are not all perfectly aligned along a "V" shape). This is likely due to the fact that the phasing between Earth and asteroids is not always optimal in the considered departure dates and transfer times. Figure 10 also shows a flyby taking place at nodal points characterised by great distances from the Earth ($r_{node} > 2$ AU).

In this case, the flyby is with a highly eccentric asteroid; the ΔV for the flyby at the node $r_{node} < 1$ AU, closer to the Earth, but also closer to the Sun, is higher, and, therefore, it is not represented in the plot. The figure shows, in fact, only the lowest ΔV solution for each asteroid.

The final asteroids shortlisted for consideration for a flyby mission scenario are reported in Table 3. The top part of the table shows the 7 asteroids with lowest ΔV and with relative velocity lower than 11.5 km/s. The bottom part of the table shows additional 4 asteroids - taken from the NASA and ESA risk list and from the database of scientifically interesting objects - with low ΔV and relative velocity. The asteroids in the NASA or ESA risk lists and those scientifically interesting, are reported with the names in bold. In particular, 2017 AB_{21}, 2004 MN_4, 2008 CC_{71}, 2000 SG_{344} and 2008 JL_3 are in the NASA or ESA risk lists while 1998 KY_{26} and 1982 DB are scientifically interesting asteroids [6]. It is worth noting how rendezvous trajectories are always significantly more expensive, mainly because of the velocity matching condition at the asteroid encounter, which requires plane change maneuvers.

Table 3: List of asteroids shortlisted for flyby missions. The table reports the name of the asteroid, its absolute magnitude H and inclination i, as well as the trajectory departure date, time of flight, the distance from the Sun of the nodal point at encounter r_{node}, the cost of the flyby ΔV, and the final relative velocity at flyby v_{rel}. In addition, the cost to rendezvous the same NEO is reported, ΔV_r.

Name	H [-]	i [deg]	T_{dep} [date]	ToF [day]	r_{node} [AU]	ΔV [km/s]	v_{rel} [km/s]	ΔV_r [km/s]
2015 KG_{158}	28.3	2.23	15/05/2030	732.3	1.0147	0.0332	7.7390	5.2580
2017 KJ_{32}	28.9	2.17	30/06/2034	690.8	1.0107	0.0381	2.6058	2.9699
2017 AB_{21}	21.0	9.91	30/09/2027	758.3	1.0019	0.0674	11.280	10.050
2004 MN_4	19.7	3.33	31/03/2027	739.9	1.0025	0.0711	5.8805	4.8848
2011 MD	28.0	2.56	31/03/2033	814.9	1.0162	0.0746	1.5949	2.0219
2007 UW_1	22.7	8.21	15/08/2025	431.7	0.9948	0.0845	4.7517	6.0194
2008 CC_{71}	24.9	1.87	31/12/2033	784.7	0.9867	0.0900	7.8612	6.4153
2000 SG_{344}	24.7	0.11	31/12/2027	638.8	0.9792	0.1584	1.5671	0.9926
2008 JL_3	25.4	0.89	31/03/2025	775.0	1.0152	0.1942	8.5293	8.6423
1998 KY_{26}	25.5	1.48	15/08/2033	772.8	1.0058	0.3515	4.3033	3.9332
1982 DB	18.2	1.43	31/12/2028	722.5	0.9714	0.4445	5.3638	5.8433

5 REMOTE SENSING ANALYSIS

We will now investigate the instruments available for a hypothetical asteroid flyby mission with the aforementioned nano-satellite, and the requirements they place on mission parameters - specifically maximum allowable closest approach distance. The mission objectives being considered will be the better determination of the target's orbital parameters by measuring its precise position and velocity relative to the spacecraft at the time of flyby, along with information on the topology of the target. The instruments being considered are a pulsed laser rangefinder (LRF) for range and Doppler shift measurements, in combination with a standard CCD camera. The LRF for ranging and Doppler measurements will be the focus of this analysis, and we will discuss qualitatively the possibility of mapping or measuring target rotation with the LRF. Kruapech and Widjaja [18] derived a formula for the collected signal power of a Gaussian beam when used in an LRF:

$$P_{ret} = \frac{T^2 \alpha \eta_{trans} \eta_{rec} D^2}{16 R^2} \left\{ 1 - exp\left[-\frac{2 r_{target}^2}{\theta^2 R^2} \right] \right\} P_{trans} \tag{10}$$

where P_{ret} is the total power collected by a detector with collecting aperture D, T is an atmospheric absorption factor which will be set to 1 in this case as this is for a space mission. α is the reflectivity/albedo of the target, η_{trans} and η_{rec} are the efficiencies of the transmitting and receiving optics

respectively, R is the range to target, r_{target} is the radius of the target (approximated as circular or spherical), θ is the beam divergence in radians, and P_{trans} is the transmitted optical power. Using this formula, an upper limit on the range for detection can be calculated by setting a lower limit on the returning power and finding the corresponding value of R.

A hypothetical asteroid and LRF were set up for use in the formula as follows. Given that the proposed spacecraft is based on the CubeSat architecture, the diameter of the receiving optic was set to 9 cm so as to fit on a single unit. The beam radius leaving the craft, w_0, was set to 1 cm given the remaining space in the corner of that unit for beam expanding optics. Beam divergence was calculated for a 1064 nm laser with 1 cm waist radius and $M^2 = 1.3$ according to $\theta = M^2\lambda/\pi w_0$, where λ is the beam wavelength and M^2 is the beam quality factor. Target albedo α was set to 0.197, which is the average for S, A and L type asteroids [19]. It is worth noting that this may be a conservative estimate, as [18] assumed isotropic diffuse reflection from the target. In the case of asteroids, the surface regolith introduces a tendency for light to be retroreflected due to the opposition effect [20], which would increase the apparent albedo. Target radius was set to 500 m, and η_{trans} and η_{ret} were left as in [18]: 0.85 and 0.45 respectively.

A conservative peak power estimate was set at 100 kW for a compact, fiber based laser system suitable for nano-satellites, with a single mode output suitable for LRF applications. Compact, all-fiber lasers with peak power outputs on the scale of hundreds of kilowatts using tens of watts of pump power have been demonstrated [21] and such a laser for space applications is currently under development at the University of Strathclyde. Assuming further design optimization and deployable solar panels on our 12U CubeSat model providing around 100-200 W, laser peak power in the region of 1 MW appears to be a reasonable upper estimate of what could be achievable. This estimation is based on commercially available deployable CubeSat solar panels.[11]

5.1 Parametric Analyses

Equation 10 was used to plot the returning signal as a function of range. Avalanche photodiodes with minimum detectable powers in the range of 1-10 nW are commercially available, so the lower limit on P_{ret} was set to 5 nW. In order to recover any Doppler shift information for relative velocity or rotation broadening, a spectral measurement device such as a scanning Fabry-Perot interferometer (SFPI),which have recently been demonstrated to work for pulsed lasers [22], must be included in the system. This must have its own dedicated photodiode, as the measurements must be done simultaneously since there is an extremely limited, non-repeatable measurement window in an asteroid flyby mission. Thus the minimum power for detection of both range and Doppler information would be at least double that for just range, i.e. 10 nW. For the case of no SFPI, with the parameters listed the maximum range for a detectable signal to be collected, R_{max}, was found to be 27.6 km. When an SFPI is included, this falls to 19.5 km.

Building on this, the effect of varying a number of parameters on R_{max} and P_{trans} was investigated. The parameters were chosen so as to help guide LRF system design and mission planning. Other parameters were left the same as the model LRF and asteroid set up previously. Firstly, it was found that reducing the target radius has no effect on R_{max} until a target radius of about 5 m is reached. This is because the beam is so tightly collimated due to the relatively large diameter on transmission that it is still smaller than the target even at distances of tens of kilometres, and so the entire beam is incident and no light is lost by missing the target. Secondly, the effects of varying P_{trans} and α on R_{max} were investigated, along with investigating the requirements places on P_{trans} assuming the closest approach and albedo are known.

It can be seen in Figure 11 that the target albedo has a significant effect on the requirement for LRF

[11] https://www.clyde.space/products/76-triple-deployable-solar-panels

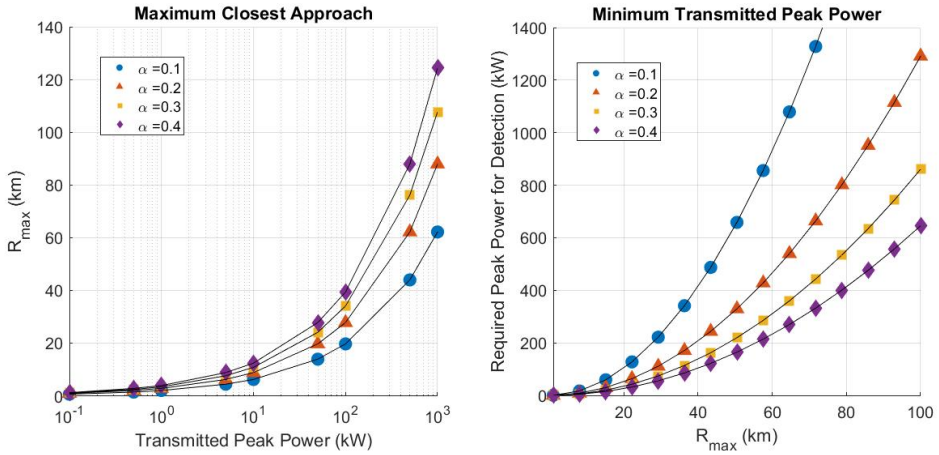

Figure 11: Left: R_{max} as a function of P_{peak}. Right: P_{peak} required for a given closest approach

peak power and the closest approach. Finally, analysis of the range limit as a function of target albedo was performed for both the case with and without and SFPI. This is shown in Figure 12. Values can be read off for potential targets; for example for S-type asteroids, one can assume an average albedo of around 0.25, which gives a maximum range of approximately 22 km and 31 km for the SFPI and no-SFPI cases.

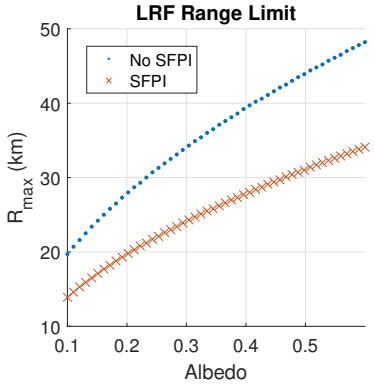

Figure 12: Maximum LRF range as a function of target albedo

5.2 Mapping and Rotation Measurements

It is possible for an LRF to also produce topographical maps of a target, by scanning the beam over the target and precisely recording the range for each point on the surface. This has been done in many orbiter missions before (MGS-MOLA, NEAR-NLR, MLA, LOLA). Rotational information could also theoretically be recovered by looking at the Doppler broadening of the returned laser signal spectrum. However, the case of an asteroid flyby places restrictions that make these types of measurement more challenging to achieve than in a rendezvous mission.

Topographic mapping with an LRF requires extremely precise and relatively slow beam-steering optics in order to scan the beam over the surface. At the time of closest approach, the relative velocities will be far too high (km/s) to scan over the target for mapping. Doing this from further away - on approach or retreat - may be possible if the target is large enough (1 km diameter asteroid at 100 km has an angular size of 0.57^o), however looking at the previous results from this study (Figure 11) this would require a peak power of ≈ 1.3 MW for $\alpha \approx 0.2$. Beam diameter at that distance would still be small enough to provide a good resolution (8.8 m). In this case, the limiting factor for lateral

resolution would be the beam divergence, as steering mirrors are available with precision on the μrad scale, which is smaller than the beam divergence ($8.8 \cdot 10^{-5}$ rad).

Doppler broadening information would only be achievable at larger ranges from the target. At close range, the beam would not cover a large enough portion of the target to be measurably broadened. The beam would have to be made more divergent in order to cover the whole target at a large range, which would mean that apart from a short time where the beam divergence and angular size are approximately equal, a significant portion of the beam would miss the target and so the signal would be too weak to be detected. Rather than broadening, a better approach would be to measure the Doppler shift on approach while doing the aforementioned scanning for mapping. This would provide a map of line-of-sight velocities which could be translated into a rotation state. Just as before however, this would require a larger peak power ≈ 1.3 MW in order to detect the signal from 100 km.

However, currently it is possible to infer some limited information about target topology using a standard CCD camera; if the lighting conditions are known, shadows can be used to reconstruct the topology to some extent.

6 CONCLUSION

This paper presented an analysis of potential missions to NEOs, using a 12U nano-satellite and low-thrust propulsion. Two scenarios, rendezvous and flyby, have been considered. The analysis of the rendezvous has been performed over 7310 NEOs using the spherical shaping method. The results of the shaping method have then been optimised with a direct method that implements a single shooting transcription of the optimal control problem. In order to study the impact of the system parameters (mass, thrust and specific impulse) on the set of reachable asteroids, a sensitivity analysis has been carried out on the entire database of rendezvous. Subsequently, a more detailed uncertainty study has been performed for asteroid 2000 SG_{344}. For the flyby scenario, 677 asteroids have been evaluated. Results have confirmed that flyby missions can be realised with a lower ΔV than rendezvous missions, making missions to highly eccentric and highly inclined NEOs feasible. The remote sensing analysis for the flyby scenarios allows us to conclude that in this proposed flyby mission, an LRF would be capable of measuring rotation and mapping topology, but only if a laser peak power of around 1.3 MW could be achieved within the CubeSat power budget. This value is beyond what has currently been achieved to the best of the authors' knowledge, but is not far off and may be possible in the near future.

7 ACKNOWLEDGEMENTS

This work was partially funded by the European Commissions H2020 programme, through the H2020-MSCA-ITN-2016 UTOPIAE Marie Curie Innovative Training Network, grant agreement 722734.

8 REFERENCES

[1] Gonzales J.A., Bello M., Martin-Albo J.F. and Galvez A., *Don Quijote: An ESA mission for the assessment of the NEO threat*, International Astronautical Congress, Paper IAC-04-Q.P.21, October 2004.

[2] Izzo D., de Negueruela C., Ongaro F. and Walker R., *Strategies for Near Earth Object Impact Hazard Mitigation*, 15th AAS/AIAA Space Flight Mechanics Conference, 23-27 January 2005.

[3] Landis G., Oleson S., McGuire M., Burke L., Martini M.C., Fittje J.E. and Packard T.W., *A Cubesat Asteroid Mission: Propulsion Trade-offs*, 50th AIAA/ASME/SAE/ASEE Joint Propulsion Conference, 2014.

[4] Woeppel E., Ott M. and Balsamo J., *The Neart Earth Object Scout Spacecraft: A Low-Cost Approach to In-Situ Characterization of the NEO Population*, SpaceOps 2014, 5-9 May 2014.
[5] Vasile M., *Robust mission design through evidence theory and multiagent collaborative search*, Annals of the New York Academy of Sciences, vol. 1065, 152–173, 2005.
[6] Perozzi E., Rossi A. and Valsecchi G.B., *Basic targeting strategies for rendezvous and flyby missions to the near-Earth asteroids*, Planetary and Space Science, vol. 49, 3–22, 2001.
[7] Novak D. and Vasile M., *Improved shaping approach to the preliminary design of low-thrust trajectories*, Journal of Guidance, Control, and Dynamics, vol. 34(1), 2011.
[8] Wlodarczyk I., *The Potentially Hazardous Asteroid 2000 SG344*, Open Astronomy, vol. 25(2), 2017, doi:10.1515/astro-2017-0120.
[9] Bombardelli C., Urrutxua H., Galvez A. and Carnelli I., *The SIROCO Asteroid Deflection Demonstrator*, Proceedings of the 22nd AAS/AIAA Space Flight Mechanics, vol. 143, 1883–1892, 2012.
[10] García Yárnoz D., Sanchez J.P. and McInnes C.R., *Easily retrievable objects among the NEO population*, Celestial Mechanics and Dynamical Astronomy, vol. 116(4), 367–388, Aug 2013, ISSN 1572-9478, doi:10.1007/s10569-013-9495-6.
[11] Di Carlo M., Romero Martin J.M. and Vasile M., *CAMELOT: Computational-Analytical Multi-fidElity Low-thrust Optimisation Toolbox*, CEAS Space Journal, vol. 10, 25–36, 2018, doi:10.1007/s12567-017-0172-6.
[12] Zuiani F. and Vasile M., *Extended analytical formulas for the perturbed Keplerian motion under a constant control acceleration*, Celestial Mechanics and Dynamical Astronomy, vol. 121, 275–300, 2015, doi:10.1007/s10569-014-9600-5.
[13] Hongmei C., Mascagni M. and Warnock T., *On the optimal Halton sequence*, Mathematics and computers in simulation, vol. 70(1), 9–21, 2005.
[14] Mehl C.H., *P-boxed for cost uncertainty analysis*, Mechanical Systems and Signal Processing, vol. 37, 253–263, 2013.
[15] Vasile M. and Tardioli C., *On the use of positive polynomials for the estimation of upper and lower expectations in orbital dynamics*, Stardust Conference, ESA/ESTEC, Noordwijk, The Netherlands, November 2016.
[16] Patterson T., *The optimum addition of points to quadrature formulae*, Mathematics of Computation, vol. 22(104), 1968.
[17] Greco C., *Variational Multiple Shooting: Theory and Applications*, Master's thesis, Delft University of Technology, 2017.
[18] Kruapech S. and Widjaja J., *Laser range finder using gaussian beam range equation*, Optics and Laser Technology, vol. 42, 749–754, 2010.
[19] Pravec P., Harris A.W., Kusnirak P., Galad A. and Hornoch K., *Absolute magnitudes of asteroids and a revision of asteroid albedo estimates from WISE thermal observations*, Icarus, vol. 221, 365–387, 2012.
[20] Belskaya I.N. and Shevchenko V.G., *Opposition effect of asteroids*, Icarus, vol. 147, 94–105, 2000.
[21] Shi W., Fang Q. and Fan J., *700-kW peak power monolithic nanosecond pulsed fiber laser*, 2014 Conference on Lasers and Electro-Optics (CLEO) - Laser Science to Photonic Applications, 1–2, 2014.
[22] Xue J., Chen W., Pan Y., Shi J., Fang Y., Xie H., Xie M., Sun L. and Su B., *Pulsed laser linewidth measurement using Fabry Perot scanning interferometer*, Results in Physics, vol. 6, 698–703, 2016.